Linear Stability Analysis of Two-Layer Rectilinear Flow in Slot Coating

Jaewook Nam
Coating Process Fundamentals Program, Dept. of Chemical Engineering and Materials Science, University of Minnesota, Minneapolis, MN 55455

Marcio S. Carvalho
Dept. of Mechanical Engineering, Pontifícia Universidade Católica do Rio de Janeiro, Rua Marques de Sâo Vicente 225, Gávea, Rio de Janerio, RJ 22453-900, Brazil

DOI 10.1002/aic.12172
Published online January 20, 2010 in Wiley Online Library (wileyonlinelibrary.com).

Two-layer coating occurs in many products. Ideally, the liquids are deposited onto the substrate simultaneously. In the case of two-layer slot coating, the interlayer between the coating liquids is subjected to enormous shearing. This may lead to flow instabilities that ruin the product. It is important to map the regions of the parameter space at which the flow is unstable. Most of the stability analyses of two-layer rectilinear flow consider the position of the interlayer as an independent parameter. Classical results cannot be applied directly in coating flows. We present a linear stability analysis of two-layer rectilinear flow considering the flow rates as an independent parameter. The predicted neutral-stability curves define the region of stable flow as a function of the operating parameters. The range of coating operating conditions is restricted further, when the condition for the desirable interlayer separation point location are considered together with the stability condition. © 2010 American Institute of Chemical Engineers *AIChE J,* 56: 2503–2512, 2010

Keywords: coating process, fluid mechanics, laminar flow, linear stability analysis, multiphase flow, mathematical modeling, films

Introduction

Continuous liquid coating is the main manufacturing step of different products, such as specialty paper, optical films and flexible electronics. It is also a very strong candidate for mass production of nanoparticle assembly films at lower cost, as discussed by Maenosono et al.[1] Most of the time, these products have more than one layer. The most efficient way to manufacture multilayer structures is to coat multiple layers simultaneously before they are solidified.

Slot coating can be adapted for coating two layers in what is called the *dual slot coating* method, as shown in Figure 1. The coating die has two separate feed slots through which each layer is fed. The flow can be divided into three regions separated by feed slots: upstream gap, mid gap, and downstream gap. When both liquids are immiscible, they form an interlayer inside the coating bead. In several coating applications, both layers use solvents that are miscible and the apparent interface is truly an inter-diffusion zone. However, it is so thin that it can be considered as a distinct interlayer with zero interfacial tension.

Previous researches about dual slot coating method were focused on controlling interlayer separation point.[2,3] When the interlayer separation point (see Figure 1) transits from the downstream corner of the mid-lip to the upstream corner, the top coating layer can invade the mid-gap region accompanied by a dangerous turn-around flow or sometimes the appearance of microvortex that may lead to coating defects. This event is called mid-gap invasion. Nam and Carvalho[3] found that when the bottom layer wet thickness $h_{w,2}$ is

Correspondence concerning this article should be addressed to M. S. Carvalho at msc@puc-rio.br.

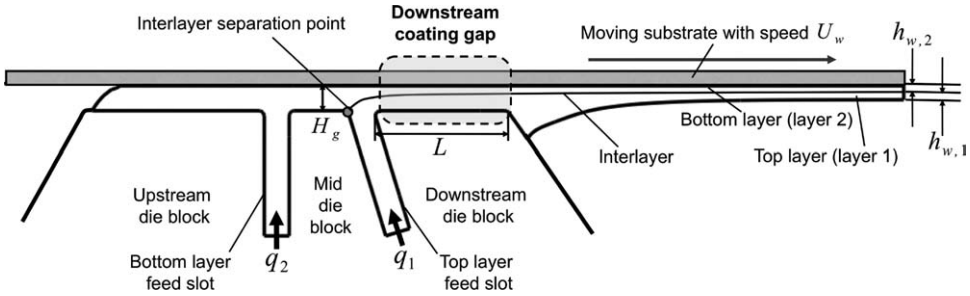

Figure 1. Two layer slot coating flow. H_g, L, U_w, $h_{w,1}$, and $h_{w,2}$ are gap height, downstream die lip length, web speed, layer 1 wet thickness, and layer 2 wet thickness, respectively.

Note that the flow rate is the product of web speed and wet thickness in slot coating process: $q_1 = h_{w,1}U_w$ and $q_2 = h_{w,2}\,U_w$. Flow region inside dotted box is called downstream coating gap.

greater than one-third of gap height H_g, mid-gap invasion can be prevented.

Even if the separation point is located at the downstream corner of the mid-lip, coating defects associated with instabilities on the interlayer may occur. A waviness in the interlayer can cause quality degradation even when the gas/liquid interface is uniform, especially for optical products. The interlayer stability can be determined at the downstream coating gap (see Figure 1), where flow under the downstream lip is almost rectilinear. In this region, the distance between the downstream die lip and moving web is about 100 μm and speed of web is about 1 m/s. Therefore, the interlayer suffers from enormous shear that may lead to the unstable configurations.

Historically, Yih[4] shows that viscosity difference, even in low Reynolds number flow, can generate instabilities along the interlayer, so called the interfacial mode in a plane Couette-Poisuille two-layer channel flow. Extensive studies about the interfacial mode on parallel channel flow has been carried out by many researchers, as Yiantsios and Higgins[5] for a pure Poiseuille flow; and Hooper and Boyd[6] and Renardy[7] for a pure Couette flow. Beside the interfacial mode, shear mode instability can be manifested by Tollmien-Schlichting waves near the wall of the channel. However, the shear mode appears only at high Reynolds number.[5] In a liquid/liquid two phase system, the viscosity difference is not the only mechanism that drives interfacial instability. Density difference can also create Rayleigh-Taylor type instability that is driven by the gravity action perpendicular to the flow direction,[8] and also a gravity-induced instability driven by the gravity action parallel to the flow direction.[9] One can find an extensive summary about two-layer flow stability in Joseph and Renardy.[10] They pointed out that long-wave disturbance at the interlayer can be suppressed by *thin-layer effect*[11] and short-wave disturbance can be damped out by interfacial tension.

Typically, the flow under the downstream die-lip in a two-layer slot coating has small channel height and high web speed, and the two-layer products usually use same or similar solvents for both layers. The flow can be characterized as a low Reynolds number with high shear flow with negligible gravitational and density difference effects. Therefore, the interlayer instability is mainly driven by viscosity difference combined with the high shear rate, not by density discrepancy.

The available analysis of two-layer rectilinear flow stability use the interlayer position as the independent parameter. In coating flows, what is fixed is the flow rate of each layer; the interface position varies as the other operating parameters are changed. Therefore, the classical results in the literature cannot be applied directly to determine the interlayer stability in two-layer slot coating.

In this study, we use linear stability theory to analyze the stability of the interlayer inside the high shear zone of a dual slot coating system: the downstream coating gap. The eigenspectrum for the flow system is computed using an efficient numerical method based on Valerio et al.[12] To find the stable region of operating conditions, we choose flow rate ratio as the flow parameter that can be controlled directly, instead of thickness ratio. Combined with viscosity ratio, the parameter ranges that guarantee linearly stable coating flow are found. Furthermore, the critical mid-gap invasion condition[3] is also considered together with the stability criteria to define the operating window of the process.

Linear Stability Analysis of Viscous Coating Flow

Formulation of equations

We consider a parallel channel to represent the two-layer flow inside the downstream coating gap as shown in Figure 2.

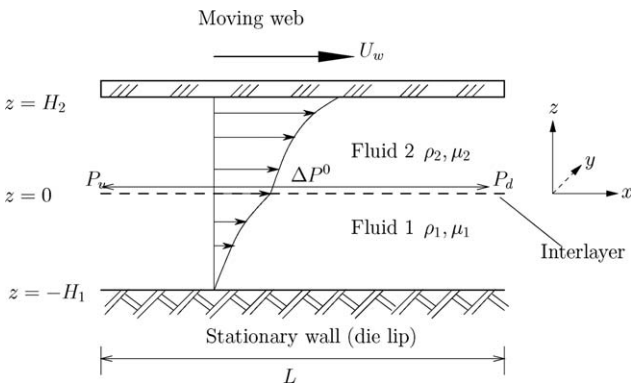

Figure 2. Base flow configuration for the downstream coating gap flow.

The system consist of two fluids with the interlayer, moving substrate and stationary wall. P_d and P_u are the downstream and upstream pressure, $\Delta P = P_d - P_u$ is the pressure difference across the flow domain, and L is the channel. With the pressure gradient across the system, the base flow profile is the combination of Couette and Poisuille flow.

The flow system consists of a moving substrate and a stationary wall where the no-slip condition applies. The pressure gradient along the channel $G \equiv \Delta P/L$, where L is the channel length, is a function of liquid properties and operating conditions. The base flow configuration have a flat interlayer at $z = 0$ with interfacial tension σ_I. Velocity and shear stress should be continuous across the interlayer, and normal stresses are balanced at it. The Layer 1, the top layer of the coating, occupies $-H_1 \le z \le 0$ and the Layer 2, the bottom layer, occupies $0 \le z \le H_2$, respectively. Fluid in layer l has density ρ_l and viscosity μ_l, and each of them is governed by the Navier-Stokes and the continuity equation.

When we use dimensionless numbers as defined in Table 1, the base flow velocity profile for layer l is

$$U_l^b(z) = \frac{1}{2\,\mu_l} G z^2 + A_l z + B_l \quad l = 1, 2, \tag{1}$$

where A_l and B_l are the coefficient,

$$A_1 = \frac{U_w}{(m+n)H_2} + \frac{1}{2}\frac{G H_2^2}{\mu_1}\frac{(n^2-m)}{(m+n)H_2} = m A_2$$

$$B_1 = \frac{U_w n}{(m+n)} - \frac{1}{2}\frac{G H_2^2}{\mu_2}\frac{(n^2+n)}{(m+n)} = B_2.$$

The goal of linear stability analysis is to determine whether the flow is stable or not with respect to infinitesimal disturbances. The perturbed fields and interlayer are written as the sum of the base states and infinitesimal disturbances:

$$\begin{aligned} \mathbf{u}_l^p(\mathbf{x}, t) &= \mathbf{i}\, U_l^b(\mathbf{x}_0) + \epsilon\, \hat{\mathbf{u}}_l \\ P_l^p(\mathbf{x}, t) &= P_l^0(\mathbf{x}_0) + \epsilon \hat{P}_l \\ h^p(\mathbf{x}_\Sigma, t) &= h^0(\mathbf{x}_{0,\Sigma}, t) + \epsilon \hat{h} = \epsilon \hat{h} \end{aligned} \tag{2}$$

where the superscript p stands for perturbed flow, $\mathbf{i}$ is the basis vector for x direction, P_l^0 is the base flow pressure field, hat(^) stands for the magnitude of disturbance in the unit of ε from the base flow, subscript l can be either 1 or 2 depending on liquid, and subscript Σ stands for the interlayer, i.e. $\mathbf{x}_{0,\Sigma}$ is the position of the interlayer in the base flow configuration.

The perturbed flow is governed by the time-dependent Navier-Stokes/continuity equations with appropriate boundary conditions.

$$\rho_l \frac{D\mathbf{u}_l^p}{D\,t} = -\nabla P_l^p + \mu_l \nabla^2 \mathbf{u}_l^p, \tag{3}$$

$$\nabla \cdot \mathbf{u}_l^p = 0 \tag{4}$$

where D/Dt is the material derivative.

No slip condition applies to both moving and stationary walls:

$$\begin{aligned} \mathbf{u}_1^p(z = -H_1) &= \mathbf{0}, \\ \mathbf{u}_2^p(z = H_2) &= \mathbf{i}\, U_w. \end{aligned} \tag{5}$$

At the perturbed interlayer, velocity and shear stress are continuous:

Table 1. Dimensionless Variables Used in Stability Analysis

Name	Definition
Reynolds number	$N_{Re} = \frac{\rho_2 U_w H_2}{\mu_2}$
Viscosity ratio	$m = \frac{\mu_1}{\mu_2}$
Density ratio	$r = \frac{\rho_1}{\rho_2}$
Thickness ratio	$n = \frac{H_1}{H_2}$
Dimensionless pressure gradient	$N_G = \frac{(\Delta P/L) H_2^2}{\mu_2 U_w}$
Interfacial tension number	$N_T = \frac{\sigma_I}{\mu_2 U_w}$

$$\mathbf{u}_1^p - \mathbf{u}_2^p|_{\mathbf{x}=\mathbf{x}_\Sigma} = 0, \tag{6}$$

$$\mathbf{t} \cdot \left[\boldsymbol{T}(\mathbf{u}_1^p) - \boldsymbol{T}(\mathbf{u}_2^p)\right] \cdot \mathbf{n}|_{\mathbf{x}=\mathbf{x}_\Sigma} = \mathbf{t} \cdot \nabla_{II}\sigma_I|_{\mathbf{x}=\mathbf{x}_\Sigma}, \tag{7}$$

where $\boldsymbol{T}$ is the state of stress. Note that Eq. 7 is set to zero, when the interfacial tension is uniform along the interlayer.

The normal stress is also balanced at the interlayer,

$$\mathbf{n} \cdot \left[\boldsymbol{T}(\mathbf{u}_1^p) - \boldsymbol{T}(\mathbf{u}_2^p)\right] \cdot \mathbf{n}|_{\mathbf{x}=\mathbf{x}_\Sigma} = 2H\sigma_I, \tag{8}$$

where the mean curvature at the interlayer $2H$ is given by

$$2H = \nabla_{II} \cdot \mathbf{n} = \frac{\nabla_{II}^2 h^p - (\mathbf{k} \times \nabla_{II} h^p)(\mathbf{k} \times \nabla_{II} h^p) : \nabla_{II}\nabla_{II} h^p}{\left(1 + (\nabla_{II} h^p)^2\right)^{3/2}}. \tag{9}$$

The motion of the interlayer is described by

$$w_\Sigma^p = \frac{Dh^p}{Dt} = \frac{\partial h^p}{\partial t} + u_\Sigma^p \frac{\partial h^p}{\partial x} + v_\Sigma^p \frac{\partial h^p}{\partial y}. \tag{10}$$

The linear differential equations that describes the disturbances are obtained after substituting the perturbed field onto the transient Navier-Stokes/continuity equations and boundary conditions, and neglecting terms of order higher than $\mathcal{O}(\epsilon^2)$. For example, the linear term of the perturbed Navier-Stokes/continuity equations are

$$\nabla \cdot \hat{\mathbf{u}}_l = 0 \tag{11}$$

$$\rho_l \frac{\partial \hat{\mathbf{u}}_l}{\partial t} + \rho_l\left[(\mathbf{i}U_l^b) \cdot \nabla \hat{\mathbf{u}}_l + \hat{\mathbf{u}}_l \cdot \nabla(\mathbf{i}U_l^b)\right] = -\nabla \hat{P}_l + \mu_l \nabla^2 \hat{\mathbf{u}}_l. \tag{12}$$

It follows that we can separate variables, so that the general solution of the initial-value problem is a linear superposition of *normal modes*, each of the form

$$\begin{aligned} \hat{\mathbf{u}}(\mathbf{x}, t) &= \mathbf{u}(z)\, \exp(i\alpha x + i\beta y + \omega t), \\ \hat{P}(\mathbf{x}, t) &= P(z)\, \exp(i\alpha x + i\beta y + \omega t), \\ \hat{h}(\mathbf{x}_\Sigma, t) &= h\, \exp(i\alpha x + i\beta y + \omega t), \end{aligned} \tag{13}$$

where α and β are wavenumbers of an imposed spatial periodic disturbances, and ω is the growth rate. When the real part of ω is less than zero, the flow system is stable with respect to the specified periodic disturbances.

Further simplification is possible due to Squire's theorem for a two-layer flow system.[13] According to the theorem, critical parameter values for the stability limit are completely determined by a two-dimensional perturbation. The flow system for two-dimensional disturbances can be easily obtained by setting $\beta = 0$. The governing equations and boundary conditions for the downstream coating gap flow system are summarized below. The momentum equation in the flow direction becomes equation of motion becomes

$$\omega \rho_l u_l + \rho_l (i \alpha U_l^{\mathrm{b}}) u_l + \rho_l \frac{\mathrm{d}U_l^{\mathrm{b}}}{\mathrm{d}z} w_l = - i \alpha P_l + \mu_l \left(\frac{\mathrm{d}^2 u_l}{\mathrm{d}z^2} - \alpha^2 u_l \right), \quad (14)$$

and the continuity equation becomes

$$i \alpha u_l + \frac{\mathrm{d}w_l}{\mathrm{d}z} = 0. \quad (15)$$

The no-slip condition at the stationary wall becomes

$$u_1(z = -H_1) = w_1(z = -H_1) = 0, \quad (16)$$

the no-slip at the moving web becomes

$$u_2(z = H_2) = w_2(z = H_2) = 0, \quad (17)$$

the velocity continuity at the interlayer becomes

$$u_1(z=0) + h \left.\frac{\mathrm{d}U_1}{\mathrm{d}z}\right|_{z=0} = u_2(z=0) + h \left.\frac{\mathrm{d}U_2}{\mathrm{d}z}\right|_{z=0}, \quad w_1(z=0) = w_2(z=0), \quad (18)$$

the normal stress balance at the interlayer becomes

$$\left[-(P_1 - P_2) + \left(2\mu_1 \frac{\mathrm{d}w_1}{\mathrm{d}z} - 2\mu_2 \frac{\mathrm{d}w_2}{\mathrm{d}z} \right) \right]\Bigg|_{z=0} + \left(\alpha^2 \sigma_I\right) h = 0, \quad (19)$$

the shear stress continuity at the interlayer becomes

$$\left[\mu_1 \left(h \frac{\mathrm{d}^2 U_1}{\mathrm{d}z^2} + \frac{\mathrm{d}u_1}{\mathrm{d}z} + i \alpha w_1 \right) - \mu_2 \left(h \frac{\mathrm{d}^2 U_2}{\mathrm{d}z^2} + \frac{\mathrm{d}u_2}{\mathrm{d}z} + i \alpha w_2 \right) \right]\Bigg|_{z=0} = 0, \quad (20)$$

and kinematic condition at the interlayer becomes

$$\omega h + i \alpha U_1^{\mathrm{b}}(z=0) h - w_1(z=0) = 0. \quad (21)$$

Discretization by Galerkin's method and finite element basis functions

Given a periodic disturbance α, the perturbed fields $\mathbf{u}$, P, h, and the growth rate ω can be computed by applying Galerkin's weighted residual method to Eq. 14 — 21. The weighting functions for the momentum equation ϕ_j and the continuity equation ψ_j are piecewise Lagrangian quadratic basis function and linear discontinuous basis function, respectively.

However, in this particular linearized system, the velocity continuity condition at the interlayer requires a jump of the velocity field disturbance across the interlayer, as indicated in Eq. 18. To handle it, we use two nodes at the interlayer: two degrees of freedom for the interfacial velocity component are assigned to the point, located at the interlayer. The pressure jump across the interlayer, a consequence of the normal stress balance, is fulfilled naturally by the linear discontinuous basis function. Therefore, the field variables are approximated by

$$\mathbf{u}_l = \sum_{j=1}^{2N+2} \mathbf{U}_j \phi_i, \qquad P_l = \sum_{j=1}^{2N} P_j \psi_i, \quad (22)$$

where N is the number of elements used to discretize the domain, $\mathbf{U}_j = \mathbf{i}U_j + \mathbf{k}W_j$ and P_j are the coefficients for velocity vector and pressure, respectively. $l = 1$ is for $-H_1 \le z \le 0$ and $l = 2$ for $0 \le z \le H_2$. The interlayer location h is assigned to single degree of freedom in this system. Note that, at the interlayer, the basis functions associated to the Layer 1 and the Layer 2 do not span across the other layer.

To obtain accurate predictions of growth rates and corresponding disturbed fields in cases at which the most dangerous modes are associated with disturbances at the interlayer, a fine mesh is necessary. To minimize the number of degree of freedom of the discrete system, we use a nonuniform mesh. We increase node concentration around the interlayer using stretching function.[14] However, as pointed out by Yiantsios and Higgins,[15] the mesh refinement requires special care in order to avoid erroneous conclusions. We compare the results from a fine uniform mesh (400 elements) with those obtained with a graded mesh (100 elements) to confirm that the graded mesh can give an accurate stability prediction with less computational time.

The number of algebraic equations is $6N + 5$, where N is the number of finite elements: $4N - 4$ momentum equations, $2N$ continuity equations, 4 no-slip conditions, and 5 interfacial conditions. In vector form, the set of equations is represented by $\mathbf{R}(\mathbf{c}) = 0$, where $\mathbf{R}$ is the vector of weighted residual equations and $\mathbf{c}$ consist of the coefficients of the finite element basis functions.

The set of differential equations constructed here leads to the generalized eigenvalue problem (GEVP)

$$\boldsymbol{J}\boldsymbol{c} = \omega \boldsymbol{M}\boldsymbol{c}, \quad (23)$$

where $\boldsymbol{M}$ and $\boldsymbol{J}$ are called the mass matrix and the Jacobian matrix. One can find detail method of constructing Jacobian and mass matrix in Valerio et al.[12]

Filtering eigenvalues at infinity

The mass matrix $\boldsymbol{M}$ is singular, because the continuity equation for incompressible fluid, the no-slip boundary conditions and the interfacial conditions, except the kinematic condition, have no time derivative. Thus, the number of finite eigenvalues of the generalized eigenvalue problem (23) is smaller than the dimension of the problem $6N + 5$. The missing eigenvalues are commonly referred to as *eigenvalues at infinity*, because if the mass matrix is slightly perturbed to

remove the singularity, e.g., $\boldsymbol{M}^* = \boldsymbol{M} + \varepsilon \boldsymbol{I}$, large eigenvalues appear in the spectrum, and they grow unbounded as $\varepsilon \rightarrow 0$.[12] During numerical computation of the eigenspectrum, truncation errors and round-off errors may cause perturbations of the mass matrix and lead to the eigenvalues at infinity—unrealistically large eigenvalues—of the GEVP. The method of filtering eigenvalues at infinity for the single-layer channel flow was discussed in Valerio et al.[12] Here, we expand the similar theory in order to apply two-layer case. In sum, the original GEVP, Eq. 23, can be transformed into the smaller eigenvalue problem that do not contain eigenvalues at infinity.

Flow rate ratio continuation

In two-layer slot coating, the independent flow variable is the flow rate ratio $f = q_1/q_2$ not the thickness ratio that naturally appears in the formulation. Therefore, we have to solve the eigenproblem using the flow rate as the independent parameters. However, it is extremely difficult to express a *close form* of the base flow velocity profile as a function of the flow rates and their ratio. However, at a fixed set of parameters, the thickness of each layer can be founded by solving the flow rate equations:

$$q_1 = \frac{(\Delta P/L)}{6\,\mu_1} H_1^3 - \frac{1}{2}\left(\frac{U_w}{(m+n)\,H_2} + \frac{1}{2}\frac{(\Delta P/L)\,H_2^2}{\mu_1}\,\frac{n^2-m}{(m+n)\,H_2}\right) H_1^2 + \left(\frac{U_w\,n}{n+m} - \frac{1}{2}\frac{(\Delta P/L)\,H_2^2}{\mu_2}\,\frac{n^2+n}{m+n}\right) H_1, \quad (24)$$

$$q_2 = \frac{(\Delta P/L)}{6\,\mu_2} H_2^3 + \frac{1}{2}\left(\frac{U_w}{(m+n)\,H_2} + \frac{1}{2}\frac{(\Delta P/L)\,H_2^2}{\mu_1}\,\frac{n^2-m}{(m+n)\,H_2}\right) m\,H_2^2 + \left(\frac{U_w\,n}{n+m} - \frac{1}{2}\frac{(\Delta P/L)\,H_2^2}{\mu_2}\,\frac{n^2+n}{m+n}\right) H_2. \quad (25)$$

Note that the interlayer location is not only a function of flow rate ratio but also a function of other parameters, like viscosity ratio. We use Newton's method to solve these equations to find H_2 and $\Delta P/L$ at a given set of flow parameters.

The flow rate equations, (24) and (25), allow multiple solutions. Each solution with respect to the flow rate ratio constructs a trajectory in a parameter map, so called a *solution branch*. Each branch shows different stability behavior. However, not all of them are physically acceptable, for example, complex values of pressure or interface location, or negative interface location.

To track a single branch, we deploy a method of continuation. One simple way to do this is to use the solution for the previous continuation step as a initial guess for the next step, the so called *zeroth order* continuation. Therefore, once we pick a correct initial guess for the first continuation step, the stability of the flow can be analyzed along a specific solution branch. In this study, we perform the flow rate ratio continuation keeping the total flow rate constant: the change of flow rate ratio was carried out by adjusting q_1 and q_2 simultaneously.

Table 2. Base Case Physical Parameters

Name	Base Case
Web speed (U_w)	1 m/s
Die lip length (L)	1 mm
Gap height (H_g)	250 μm
Layer 1 Viscosity (μ_1)	46 cP
Layer 2 Viscosity (μ_2)	23 cP
Layer 1 density (ρ_1)	1.2 g/ml
Layer 2 density (ρ_2)	1.2 g/ml
Layer 1 wet thickness ($h_{w,1}$)	50 μm
Layer 2 wet thickness ($h_{w,2}$)	50 μm

Here, we propose a two step method to perform the stability analysis on the flow:

1. Solving flow rate equations for each layer to find the interlayer location.
2. Converting the interlayer location to thickness ratio and use it with the conventional base flow profile to perform the linear stability analysis.

Results and Discussion

We use linear stability analysis to find the desirable operating condition ranges for the dual slot coating method. One way to visualize the stable region in the parameter space is to construct the neutral stability curve or neutral curve, by collecting neutrally stable points with respect to different flow parameters and wavenumbers. Furthermore, since our target is to find the ranges for defect-free products, the stability results obtained here are combined with the critical mid-gap invasion conditions presented by Ref. 3.

Construction of the neutral curve

The solution of the GEVP, Eq. 23, at a given set of flow parameters and wavenumber is a set of eigenpairs. Here, we use dimensionless variables based on the characteristic length unit H_g and time unit H_g/U_w to display the results. Flow parameters and operating conditions of the base are summarized in Table 2. The most dangerous eigenvalue that can lead to flow instability are those with the largest real part, or growth rate. The solid dot in Figure 3 a is the most dangerous eigenvalue at dimensionless wave number $\alpha^* = 3.80$ with the largest real part $\omega^*_{R,MD} = -5.43 \times 10^{-3}$. The corresponding eigenvectors are presented in Figures 3 b,c,d. The plots show the modulus of eigenvector components with respect to vertical coordinate z^* for horizontal velocity u, vertical velocity w, and pressure p, respectively. Note that the moduli are normalized with respect to the maximum value for each variable. The eigenvector plots show that the disturbances are concentrated near the interlayer — interfacial mode. We found that the interfacial mode is always the most dangerous disturbance for the parameter ranges considered in this study.

When we collect the most dangerous growth rate at different wavenumbers and flow parameters, two types of growth rate plots are obtained, as shown in Figure 4. Plot (a) was constructed by finding the most dangerous eigenvalue from a wavenumber range scanned over at the fixed flow rate ratio $f = 1$. We will call it wavenumber continuation. Plot (b) was

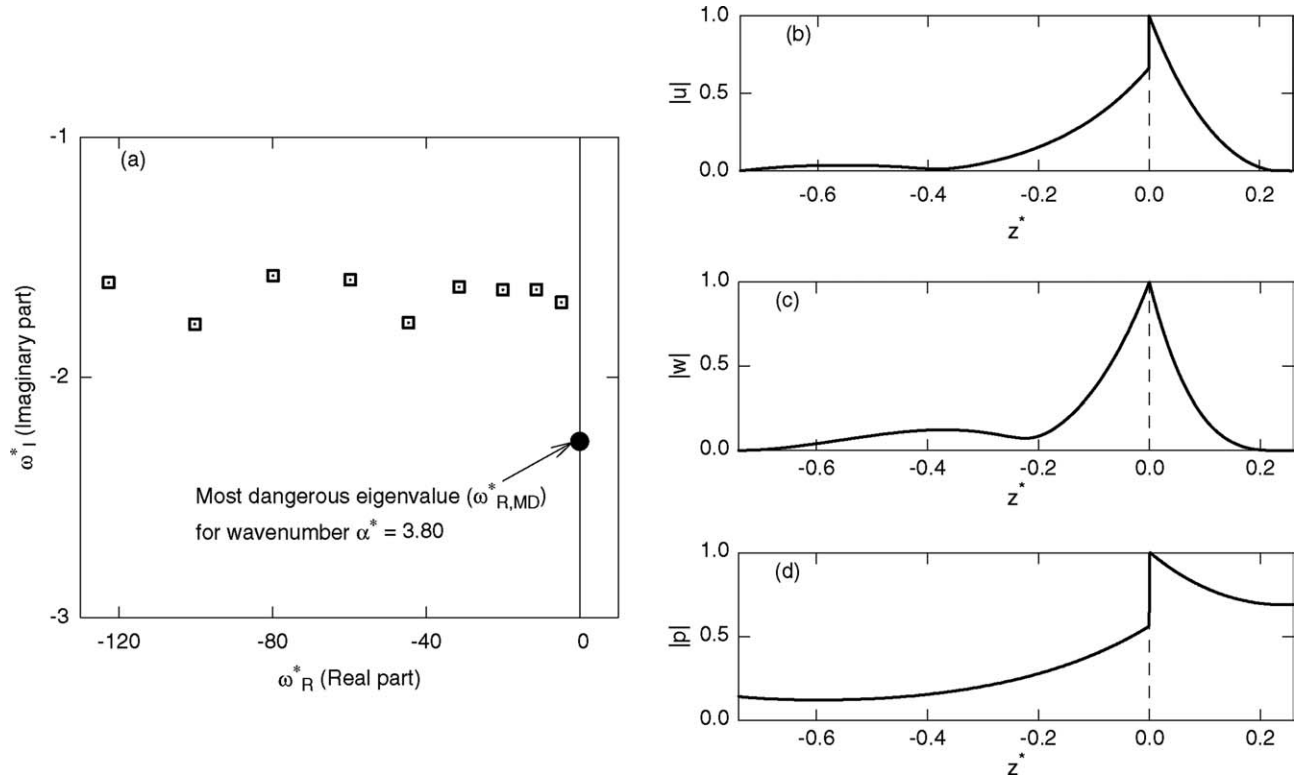

Figure 3. Results from two-layer slot coating flow stability model without interfacial tension for density ratio $r = 1$, viscosity ratio $m = 2$, flow rate ratio $f = 1$, and dimensionless wavenumber $\alpha^* = 3.80$.

(a) Shows ten loading eigenvalues from eigenspectrum. (b), (c), and (d) plot show eigenvectors corresponding to the solid dot in (a).

constructed using flow rate ratio continuation, as discussed in Flow Rate Ratio Continuation section, at wavenumber $\alpha^* = 3.8$. In both plots, the density ratio and viscosity ratio are fixed to $r = 1$ and $m = 2$. The solid dot in both plots represents to most dangerous eigenvalue of Figure 3a. The open triangle point and square point in Figures 4a,b are neutrally stable points at which the growth rate vanishes. The corresponding wavenumber and flow rate ratio are $\alpha^*_N = 6.75$ and $f_N = 0.535$, respectively. In Plot (a), the flow is linearly stable only when the wavenumber is lower than α^*_N; and, in plot (b), the flow is stable only when flow rate ratio is higher than f_N.

Neutral curves can be constructed by collecting neutrally stable points with respect to wavenumbers and flow

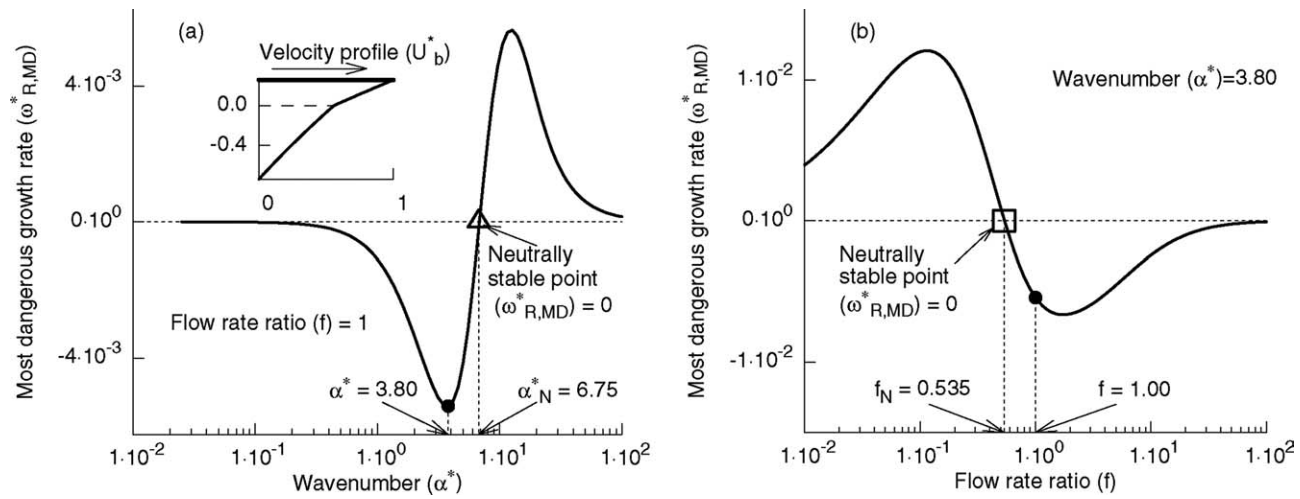

Figure 4. Most dangerous growth rate versus wavenumber plot at fixed flow rate ratio $f = 1$ (a) and Most dangerous growth rate versus flow rate ratio plot at fixed wavenumber $\alpha^* = 3.80$ (b).

Small plot inside (a) shows the base flow velocity profile for given parameters.

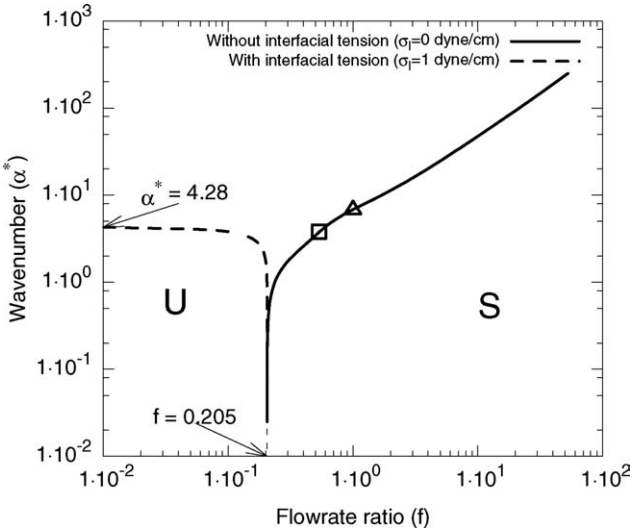

Figure 5. Neutral curve for density ratio $r = 1$ and viscosity ratio $m = 2$ with or without interfacial tension.

Interfacial tension used in this study is $\sigma_I = 1$dyne/cm. Note that triangular point and square point are neutrally stable points obtained from Figure 4a, b, respectively. "U" and "S" stand for unstable interlayer and stable interlayer, respectively.

parameters. Figure 5 shows a representative neutral curve that depicts stable and unstable region inside the parameter space of wavenumber and flow rate ratio. Neutral curve with solid line was obtained without interfacial tension, and dotted line was obtained with interfacial tension, e.g., $\sigma_I = 1$ dyne/cm.

As there is no method to track neutrally stable point, the point should be collected from scanning over ranges of wavenumber and a flow parameter. When the neutral curve is perpendicular to the flow rate ratio axis, a wavenumber continuation is the proper method to collect neutrally stable point. Flow rate continuation is used otherwise.

When the interfacial tension vanishes ($\sigma_I = 0$), there is always a range of flow rate at which the flow is unstable. However the results at high wavenumber should be analyzed with care. At $\alpha^* \gtrsim 10^2$, the wave length of the disturbance is very small, less than a micron, in the cases analyzed here. This length may be comparable to the characteristic length unit of interlayer diffusion that was neglected in our model. Therefore, without including diffusion, it is hard to determine whether the interlayer is stable or not.

When interfacial tension does not vanish, e.g., $\sigma_I = 1$dyne/cm ($N_T = 0.0435$), the tension damps out the high wavenumber disturbance: perturbations at wavenumber α^* above 4.28 are always stable. In this case, flow rate ratio above $f > 0.205$ guarantees linearly stable interlayer.

In this study, we determined neutral curves as a function of viscosity ratio and flow rate ratio to determine the desirable operating condition range.

Finding stable flow rate ratio range

Figure 6 shows the neutral curves for high viscosity ratio $m = 2$ with or without interfacial tension at different total wet thickness $h^*_{w,t}$. As shown in Figure 6b, the interfacial tension damped-out high wavenumber disturbances. However, stability characteristics of both flows, with and without interfacial tension, are the same from low to medium wavenumber range.

According to the predictions, large flow rate ratio leads to a stable interlayer at $m = 2$. The reason is that the less viscous Layer 2 becomes thin at large flow rate ratio $f = q_1/q_2$, and the thin-layer effect stabilizes interlayer disturbance as discussed in the literature. The range of flow rate ratio for stable interlayer increases as total wet thickness $h^*_{w,t} = h_{w,t}/H_g$ decrease, i.e., thinner coating is favorable in terms of the interlayer stability.

Figure 7 shows the neutral curve at viscosity ratio $m = 0.5$ at different total wet thickness. Now, Layer 1 is less viscous than Layer 2. At low and intermediate wavenumbers, the stable region is now restricted to low flow rate ratio. This is easily explained by the fact that the flow is stable when the low viscosity layer is thin.[10] The stable region shrinks as the total wet thickness $h^*_{w,t}$ falls. Therefore, in this case, thick coating favorable for interlayer stability.

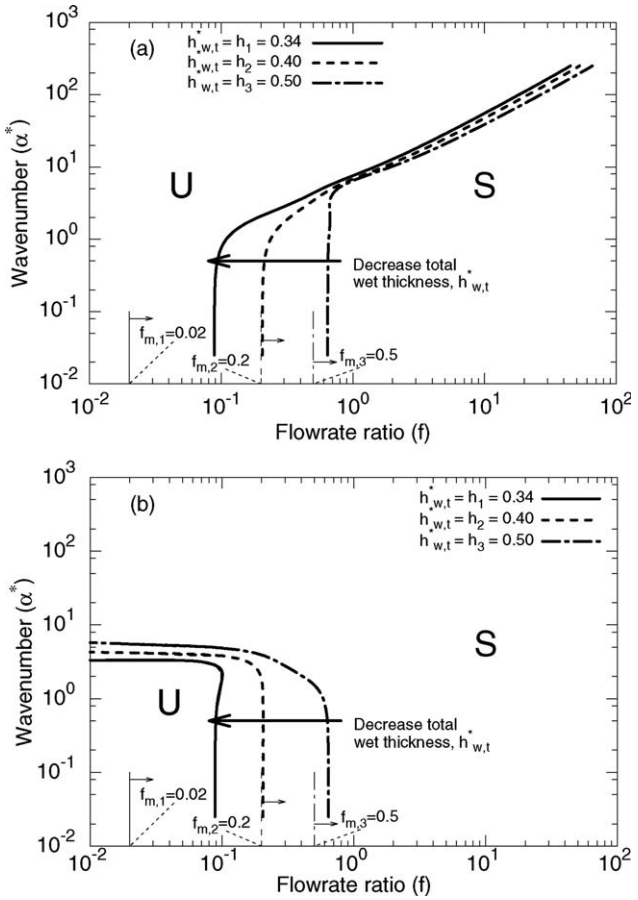

Figure 6. Neutral curve for density ratio $r = 1$ and viscosity ratio $m = 2$ with interfacial tension (a) or without interfacial tension (b) for different total wet thickness, $h_{w,t} = 0.34$, 0.40, and 0.50.

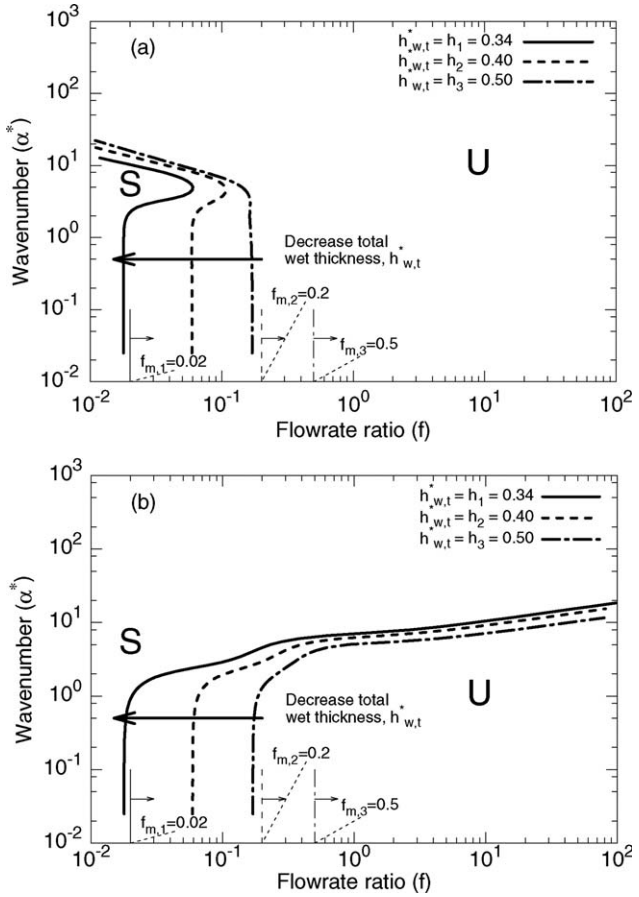

Figure 7. Neutral curve for density ratio $r = 1$ and viscosity ratio $m = 0.5$ with interfacial tension (a) or without interfacial tension (b) for different total wet thickness, $h_{w,t} = 0.34$, 0.40, and 0.50.

Critical flow rate ratio condition for mid-gap invasion

Interlayer instability is not the only source of coating defects. As discussed by Nam and Carvalho,[3] if the wet thickness of the bottom layer (Layer 2) is less than approximately one-third of the coating gap the separation point travels through the mid-lip leading to coating defects. As dual slot coating method is known as a premetered method, the thickness of the deposited liquid layer is set by the flow rate and the web speed: $h_{w,l} = q_l/U_w$, where $l = 1$ or 2. The total wet thickness $h_{w,t} = h_{w,1} + h_{w,2}$ is usually set by product specifications, therefore, the critical flow rate ratio for the mid-gap invasion can be computed from the results presented by Nam and Carvalho[3]:

$$f_m = \frac{q_1}{q_2} = \frac{h_{w,1}}{h_{w,2}} = \frac{3\,h_{w,t} - H_g}{H_g} = \frac{3q_t - H_g\,U_w}{H_g\,U_w} = 3\,h^*_{w,t} - 1. \tag{26}$$

Therefore, coating defects can be present when the flow rate ratio f is greater than the critical value f_m. Note that in this simple criterion, the critical condition does not depend on the material property like viscosity and density. This condition should be considered together with the linear stability analysis results for finding desirable operating conditions.

The predictions at high viscosity ratio ($m = 2$), Figure 6, show that the stable range of flow rate coincides with the range of flow rate at which mid-gap invasion occurs. Therefore, operation at high viscosity is not recommended when both interlayer stability and mid-gap invasion are considered simultaneously. At low viscosity ratio ($m = 0.5$), Figure 7, the stable range of flow rate is free of mid-gap invasion. Consequently, operations with the top layer less viscous than the bottom layer is recommended to prevent coating defects coming from interlayer instability and mid-gap invasion.

Finding desirable viscosity ratio range

According to the results from Critical Flow Rate Ratio Condition for Mid-Gap Invasion section, low viscosity ratio, i.e., a less viscous top layer, is favorable for interlayer stability. However, there are limits on the range of viscosity ratio that stabilizes the flow. Figure 8a shows the neutral stability curve in the plane of wavenumber and viscosity ratio at a

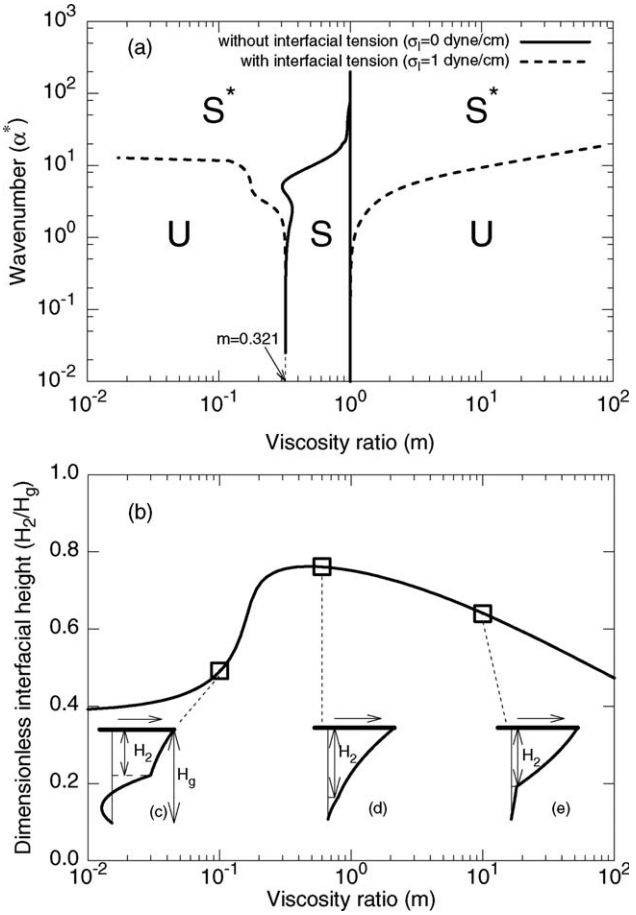

Figure 8. Neutral curve for density ratio $r = 1$, flow rate ratio $f = 0.04$, and total wet thickness $h^*_{w,t} = 0.4$ with or without interfacial tension.

"S" and "U" stand for stable and unstable interlayer, respectively. "S*" inside plot (a) stands for stable interlayer only when interfacial tension is presented. Plot (b) shows the interlayer location. Plots (c), (d), and (e) show the base flow profiles at $m = 0.1$, 0.6, and 1, respectively.

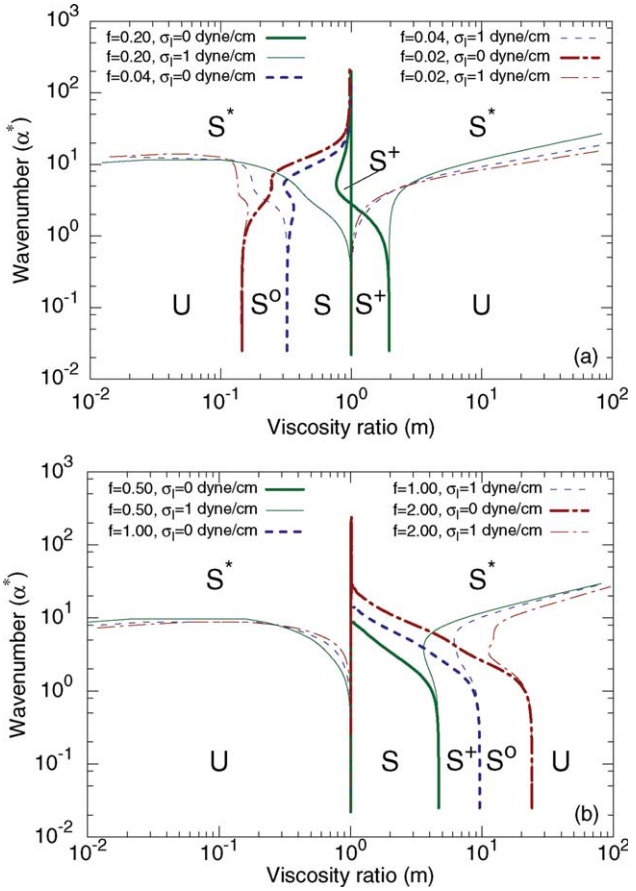

Figure 9. Neutral curve for density ratio $r = 1$ and total wet thickness $h^*_{w,t} = 0.40$ for different flow rate ratio with or without interfacial tension.

Note that when the viscosity for both layers are the same ($m = 1$), interlayer is neutrally stable because there are no distinction between layer 1 and layer 2. Plot (a) displays $f = 0.20$, 0.04, and 0.02, and plot (b) displays $f = 0.50$, 1.00, and 2.00. For plot (a), "S" is stable for $f = 0.02$ and 0.04, "S^o" is stable for $f = 0.04$, and "S^+" is stable for $f = 0.20$. For plot (b), "S" is stable for $f = 0.50$, 1.00, and 2.00, "S^+" is stable for $f = 1.00$ and 2.00, and "S^o" is stable for $f = 2.00$. "S*" inside plots (a) and (b) stands for stable interlayer only when interfacial tension is presented. [Color figure can be viewed in the online issue, which is available at wileyonlinelibrary.com.]

fixed flow rate. Note that, for the chosen flow rate ratio, $f = 0.04$, there is no mid-lip vortex and turn-around flow inside mid-gap region: no mid-gap invasion. Considering low and intermediate wavenumbers, the interlayer is linearly stable only from $m = 0.321$ to 1.00. The flow is unstable if top layer is more viscous ($m > 1$) or if its viscosity is much smaller than the bottom layer ($m < 0.321$). Again, stability of high wavenumber disturbance may not be predicted without diffusion for vanishing interfacial tension case, and the small wavelength disturbance are always faded away by the action of interfacial tension (region S*).

The existence of a range of viscosity ratio at which the flow is stable can be explained by the fact that although the flow rate ratio and total flow rate are fixed, the location of interlayer is not constant, but it is a function of viscosity ratio. Figure 8b displays the Layer 2 thickness inside the downstream coating gap region as the viscosity ratio increases. The results are based on solving Eqs. 24 and 25 at given flow rates. The less viscous layer is thin inside the range of $m = 0.321$ to 1.00. Note that, in this range, the less viscous layer is Layer 1 (the top layer). When the viscosity ratio is less than 0.321, the less viscous Layer 1 is not thin, because of turn-around flow, as shown in Figure 8c. When the viscosity ratio is greater than one, the less viscous Layer 2 is always thicker than Layer 1, as shown in Figure 8e. The results clearly show that only a limited viscosity ratio range enables the thin-layer effect that leads to stable flow.

The viscosity range for stable flow is a function of flow rate ratio. Figure 9 shows the neutral curves for different flow rate ratios at total wet thickness $h^*_{w,t} = 0.40$ and immiscible liquid ($\sigma_I = 0$). Neutral stability curves in plot (a) of Figure 9 shows that the stable regimes appear at moderately low viscosity ratio m except at $f = 0.2$. As the flow rate ratio increases, the neutral stability curves at low and moderate wavenumber, $\alpha^* = 10^{-2} - 10^1$, shift toward the high viscosity ratio. At high flow rate ratios, plot (b), the stable window occurs at a viscosity ratio range above $m = 1$.

Not all stable regimes in Figure 9 are desirable in a point of view of coating operations. When the location of the interlayer separation point is not located at the downstream corner of the mid lip (mid-gap invasion), either micro-vortex under the mid-lip or periodic oscillation of the interlayer can cause coating defects or degrade product quality.[3] At the total thickness $h^*_{w,t} = 0.40$, the critical flow rate ratio for mid-gap invasion is $f_m = 3 \times 0.40 - 1 = 0.20$. Therefore, plot (a) shows neutral curves for low flow rate ratio and they are free from mid-gap invasion. On the contrary, flow rate ratios for plot (b) implies that, even though the coating flow are linearly stable at high viscosity ratio, mid-gap invasion can cause problems in production.

Conclusion

Linear stability analysis was carried out on the two-layer flow in the downstream coating gap of a dual slot coating system. The problem is written in terms of the flow rate ratio, instead of the usual thickness ratio. The original generalized eigenvalue problem was effectively reduced to a smaller size simple eigenproblem by extending the method proposed by Valerio et al.[12] The most dangerous disturbance related to the largest real part of eigenvalue or growth rate was found to be concentrated at the interlayer. The waviness of the interlayer caused by the disturbance can spoil the quality of two-layer coating product. Therefore, it is important to find parameter ranges at which the flow is a stable to prevent coating defects.

When the neutrally stable points, where the growth rate changes sign, are computed as a function of wavenumber and flow parameters, a neutral curve can be constructed in order to mark stable and unstable regions in the parameter space. As pointed out by Joseph and Renardy,[10] the long wave (large wavenumber) disturbance can be suppressed by utilizing thin-layer effect, i.e., making the less-viscous liquid layer thin, while the short-wave (small wavenumber) disturbance is damped out by the action of interfacial tension. When miscible coating liquids are considered (vanishing interfacial tension), the stability of short wave disturbance is hard to determine without including diffusion in the model.

Besides the interlayer instability, the location of the interlayer separation point can cause coating defects.[3] The critical mid-gap invasion condition can be rewritten in terms of flow rate ratio at the fixed total flow rate or total wet thickness.

Combining the range of operating parameters for stable two-layer flow and pinned separation point (no mid-gap invasion), a defect free region can be created. The predictions show that the recommended conditions are at low flow rate ratio $f = q_1/q_2$ and low viscosity ratio $m = \mu_1/\mu_2$, i.e., a thin top layer of a low viscosity liquid. These condition exploit the thin layer effect without invoking mid-gap invasion. Because the interlayer location in the downstream coating gap is a function of the viscosity ratio at a fixed flow rate, only a small window of viscosity ratio leads to stable flows. The defect free region is a function of the total flow rate; it shrinks as the wet thickness falls.

Acknowledgments

The authors thank Prof. D. D. Joesph (Aerospace engineering and Mechanics, University of Minnesota) for suggestions and discussions about linear stability flow model. They dedicate this work to the late Prof. "Skip" Scriven. He participated in the first steps of this research and unfortunately could not see its completion.

Literature Cited

1. Maenosono S, Okubo T, Yamaguchi Y. Overview of nanoparticle array formation by wet coating. *J Nanoparticle Res.* 2003;5:5–15.
2. Taylor SD, Hrymak AN. Visualization and flow simulation of a two-layer slot coater. *Chem Eng Sci.* 1999;54:909–918.
3. Nam J, Carvalho MS. Mid-gap invasion in two-layer slot coating. *J Fluid Mech.* 2009;631:397–417.
4. Yih C. Instability due to viscosity stratification. *J Fluid Mech.* 1967;27:337–351.
5. Yiantsios SG, Higgins BG. Linear stability of plane Poiseuille flow of two superimposed fluids. *Phys Fluids.* 1988;31:3225–3238.
6. Hooper AP, Boyd WGC. Shear-flow instability at the interface between two viscous fluids. *J Fluid Mech.* 1983;128:507–528.
7. Renardy Y. Instatility at the interface between two shearing fluids in a channel. *Phys Fluids.* 1985;28:3441–3443.
8. Yiantsios SG, Higgins BG. Rayleigh-Talyor instability in thin viscous films. *Phys Fluids A.* 1989;1:1484–1501.
9. Renardy Y. Viscosity and density stratification in vertical Poiseuille flow. *Phys Fluids.* 1987;30:1638–1648.
10. Joseph DD, Renardy Y. *Fundamental of Two-Fluid Dynamics, Interdisciplinary Applied Mathematics*, Reading, MA: Springer, 1993.
11. Hooper AP. Long-wave instability at the interface between two viscous fluids: thin layer effects. *Phys Fluids.* 1985;28:1613–1618.
12. Valerio J, Carvalho MS, Tomei C. Filtering the eigenvalues at infinite from the linear stability analysis of incompressible flows. *J Comput Phys.* 2007;227:229–243.
13. Hesla TI, Pranckh FR, Preziosi L. Squire's theorem for two stratified fluids. *Phys Fluids.* 1986;29:2808–2811.
14. Vinokur M. On one-dimensional stretching functions for finite-difference calculations. *J Comput Phys.* 1983;50:215–234.
15. Yiantsios S, Higgins BG. Analysis of superposed fluids by the finite element method: linear stability and flow development. *Int J Numerical Methods Fluids.* 1987;7:247–261.

Manuscript received Oct. 1, 2009, and revision received Dec. 11, 2009.